

# Scalability, Delay Characterization, and Satisfiability of Quality-of-Information in Wireless Networks

**Abstract**—Quality of Information (QoI) provides a context-dependent measure of the utility that a network delivers to its users by incorporating non-traditional information attributes. Quickly and easily predicting performance and limitations of a network using QoI metrics is a valuable tool for network design. Even more useful is an understanding of how network components like topology, bandwidth, protocols, etc. impact these limitations. In this paper, we develop a QoI-based framework that can provide this understanding of limitations and impact by modeling the various contributors to delay in the network, including channel rate and contention, competing traffic flows, and multi-hop propagation effects, and relating them to QoI requirements, especially completeness and timeliness. Analysis shows that large tradeoffs exist between network parameters, such as QoI requirements, topology, and network size. Simulation results also provide evidence that the developed framework can estimate network limits with high accuracy. Finally, this work also introduces *scalably feasible QoI regions*, which provide upper bounds on QoI requirements that can be supported for certain network applications.

## I. INTRODUCTION

Traditional approaches to studying network scalability and performance limitations have been focused on finding theoretical limits on throughput and delay. In many applications, however, the relationship between these metrics and the effectiveness of the network is highly non-linear. Therefore, having a framework to evaluate network scalability with respect to achievable *Quality of Information* (QoI) requirements is necessary.

Additionally, while theoretical, asymptotic analysis of individual network topologies, protocols, etc. is important, such analysis lacks the ability to quickly obtain an accurate estimate of a projected network's abilities when these individual components are pieced together. Often, extensive simulation or experimentation testbeds must be created to test proposed network setups, which is difficult and time-consuming.

As an example, imagine being given the task of deploying a wireless sensor network for a particular application. Given a proposed network with a defined size, topology, parameters, and protocols, what is the level of QoI requirements it can support? Now, consider the converse: Given a certain QoI that is desired by users of a network, what is the maximum number of nodes that the network can support? Which has a bigger impact on this scalability, the imposed information requirements, or the strict timeliness requirements?

To provide answers to questions like these, our main contribution in this paper is a novel framework that can predict scalability and performance of a network with respect to QoI requirements, explained in detail in Section IV. We

first present an example of an application that relies on QoI to highlight the difference in QoI and traditional metrics in Section III. The framework is validated with simulation results in Section VII. We also show in Section IX that this model is also quite useful in quickly and easily understanding the impact of parameters and design choices, providing a secondary benefit to network designers of allowing them to compare networks and identify tradeoffs. Finally, we show how the framework can also provide bounds on QoI capacity in some applications in Section X.

## II. RELATED WORK

The scalability model derived in this work is inspired by the asymptotic scalability framework outlined in [1], which has been previously applied to content-agnostic static networks [2] and mobile networks [3]. Other works characterize the capacity of wireless networks, like [4], [5], but all do so by considering how networks scale asymptotically or by analyzing specific network instances instead of developing a general model. Experimental techniques, like Response Surface Methodology [6], for example, may be applied to solve the problem we do, but these require complex test beds instead of a compact mathematical framework.

A large number of works provide definitions for QoI and frameworks that utilize it. We will address only the most relevant ones here. Primarily, QoI has been considered from a number of various angles including routing [7], scheduling/rate control [8], [9], and impact on usage of network resources [10]. Our focus is on a broader scale here, though, modeling scalability and limitations of an entire network.

A framework called Operational Information Content Capacity is outlined in [11], which describes the obtainable region of QoI, a notion similar to the *scalably feasible QoI region* developed here. This approach does not provide any method for determining the possible size of the network or impact of network design choices like medium access protocols. We also note that a notion similar to QoI satisfiability was considered in [12] which addresses resource allocation for long-term average QoI outage satisfaction. However, the focus of [12] is energy-efficient scheduling and power allocation in a single-hop three-node network rather than scalability.

In Section III, we use similarity-based image collection as an example of an application that is best evaluated using QoI. This application has previously been considered in [13] and [14]. Our scope is greater than that of [13], which does not consider attributes of timeliness, nor the consideration of transmission rates and network topology. We use the same

similarity-based image selection algorithm as in [14], but provide new methods of quantifying QoI.

### III. QOI MODEL

QoI is a multi-dimensional metric that can be defined for an application to give a more meaningful measure of the value of information. It consists of attributes such as timeliness, freshness, completeness, accuracy, precision, etc. For example, information that contributes to a decision-making process may only be useful if it arrives before the decision must be made, or it may have varying usefulness based on how similar or dissimilar it is to other data already collected.

The specific details of which attributes are considered and how they contribute to QoI is application-dependent. Chosen QoI metrics are stored as a vector associated with a data item. Here, as in [15], we specify a vector of minimum values for each QoI metric, and data is evaluated based on whether it satisfies all of the QoI requirements or not. We use this approach to establish the edges of QoI satisfiability for the vector of metrics, which defines the boundaries of maximum achievable QoI regions in the metric space.

We choose to use two QoI attributes, one that is time-based and one that is information-content-based. The first attribute is timeliness,  $T$ , of data. For the second attribute, we present a notion of *completeness*,  $C$ , which we show can be defined multiple ways, depending on the application and context. Together, a QoI requirement of  $\mathbf{q} = \{C, T\}$  specifies a quantity of data that must be delivered as well as a deadline by which it must arrive to be useful. Since completeness is a new concept, we explain an example image selection algorithm and show how it can be evaluated with completeness.

#### A. Example Application: Similarity-based Image Retrieval

As a motivating example, we choose a network in which nodes store photographs that are to be exchanged or collected at one or more data sinks. This example covers surveillance missions of military tactical networks or camera sensor networks.

Each of these queries require measuring the similarity or dissimilarity of two images. To get a similarity measurement, we use the same choice as was shown to be effective in [14]. A technique called Color and Edge Directivity Descriptor (CEDD) [16] provides a 54-byte vector of qualities inherent to a photograph like lightness, contrast, and color. The similarity between two images can then be given as a scalar by calculating the *Tanimoto Similarity* [17] between their CEDD vectors. Dissimilarity is simply defined as 1 minus the similarity.

1) *Selecting Similar Images*: One possible query for data is to retrieve images from the network that are similar to an identified target image. The first type of query we introduce occurs when a user already has one image of a particular area or object of interest and would like to obtain similar images to get a more complete view of that specific scene or object. For example, if a user has a picture of an unknown suspicious person entering a building, but the person is not identifiable from that image, it would be useful to collect more images

that are similar to that one with the possibility that another picture may have a better view of the person in question that can be used for identification or more context. Called **Top-K**, the query algorithm used for this application will choose the  $k$  images with the most similarity with respect to the target image.

We can evaluate the completeness of the result in one of two ways. First, we can use the similarity of the images as a value representing each image's effectiveness in providing a more complete view of the target scene. If we sum the similarity of all  $k$  images returned by the algorithm, we get a representation of completeness, which we naturally call *Sum Similarity*. While this measure of completeness is abstract, it can be refined in an actual implementation through testing and evaluating. This definition of completeness is useful, though, because it can be applied without any predetermined knowledge of the environment or pool of images. Second, if the environment is able to be partitioned into  $n$  distinct area or settings, then completeness can be defined as the fraction of received images that are in the same set as the target image.

Often, though, we can partition the environment in which the network operates into a number,  $n$ , of distinct settings or areas. In those cases, we can utilize a second method of quantifying completeness. Assume that each image belongs to one of these  $n$  sets, related to the setting it depicts. Naturally, then, when executing a Top-K query, the goal is for the algorithm to return images from the same set as the target image. Completeness can then be given by the fraction of images returned that are in the same set as the target image.

2) *Selecting Diverse Images*: In contrast, given the set of all photographs available in the network, we might want to return the set of  $k$  images that exhibits the most diversity, ideally providing a user with a good sampling, or *complete view*, of available images. For instance, such a result would be quite useful in a surveillance mission. We present two query algorithms that can be used to achieve this goal.

One query that provides diverse images is known as the **Spanner** of the set of known photographs. For the Spanner algorithm, we employ a greedy algorithm similar to that in [14]. Here, the algorithm simply chooses images that provide the greatest minimum distance from all images already chosen. This minimum distance can be added to a running sum to provide a completeness metric of *Sum Dissimilarity*. This value represents a measure of completeness because a higher level of dissimilarity provides a more complete view of the feature space. To simplify implementation and to define a *Sum Dissimilarity* metric. Here, the algorithm first chooses the two images with the greatest dissimilarity between them from all available images. Then, each successive image is chosen to be the one with the greatest minimum distance between it and all images already chosen, until  $k$  images are selected. This minimum distance between the image being selected and the images in the collected set is the value added to the running cumulative completeness metric of *Sum Dissimilarity*. Since the Spanner algorithm's goal is to provide images at the edges of the available feature space, the Sum Dissimilarity

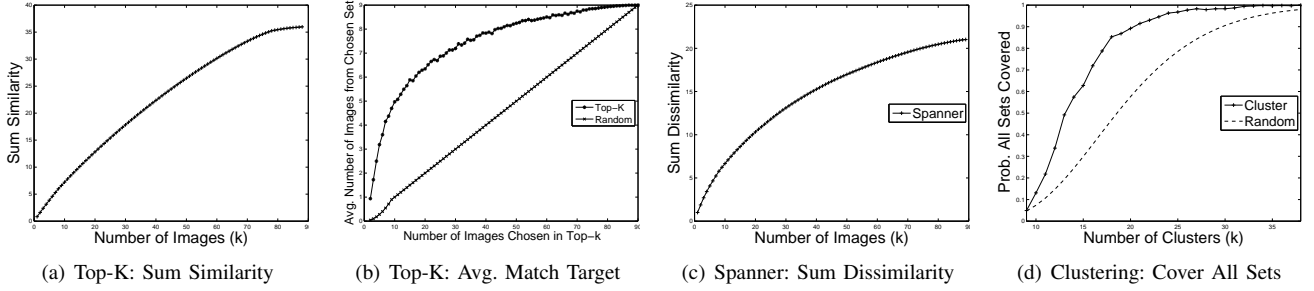


Fig. 1. Completeness metrics for the three image selection algorithms. Each exhibits a diminishing return as more images are added.

represents a measure of its completeness because a higher level of dissimilarity is providing a more complete view of the feature space.

The other query that can achieve a complete view over all images is **Clustering**. In the Clustering algorithm, all images are separated into a  $k$  clusters based on their pairwise distances using any version of a  $k$ -means clustering algorithm, where  $k$  is given by the user. Then, the most central image from each cluster is returned. Here, assuming that the photographs of the same settings or objects of interest exhibit similar characteristics, Clustering also provides a complete view of the network's environment.

Both Spanner and Clustering algorithms can also be evaluated using a model assuming the environment is split into  $n$  sets. With this model, we can define completeness as either the number of sets represented by at least one of the  $k$  images returned or the probability of all  $n$  sets being represented by at least one image when  $k$  are returned. Here, though, we only show results for the second definition.

### B. Experimental Results

To provide example values of these completeness metric definitions, experiments applying this query algorithm were run on a set of pictures taken at  $n = 9$  different settings around the Penn State campus. The algorithm was run 1,000 times on a random sampling of 90 images in each trial. Average results for the sum similarity of received images is shown in Figure 1(a) and the number of received images that match the target is shown in Figure 1(b) each completeness metric are shown in Figure 1.

To provide example values of these completeness metric definitions, experiments applying each query algorithm were run on a set of pictures taken at  $n = 9$  different settings around the Penn State campus. Each of these 9 settings is of a pictorially different area, e.g. a particular building, a downtown street, or a lawn setting, and over 20 images of each was taken. Then, for individual trials, 10 images from each set were randomly selected to create an image pool of 90 pictures. The three algorithms were run over these 90 images, with the target image being randomly selected in the case of Top-K. Results for each of the different completeness metrics were averaged over 1,000 trials are shown in Figures 1(a) to 1(d).

Figure 1(a) shows the average sum similarity of images returned by the Top-K algorithm. Figure 1(b) provides the

second definition of completeness for the Top-K algorithm, the number of images matching the set that the target image was randomly chosen from. Completeness results when dissimilarity is the objective are shown in Figures 1(c) and 1(d). Specifically, Figure 1(c) depicts the average Sum Dissimilarity returned by the Spanner algorithm, and Figure 1(d) represents the empirical probability of all 9 sets being represented in the  $k$  returned images. For reference, we also include expected values for the metrics in Figures 1(b) and 1(d) if the images were selected from the entire image pool at random, i.e., without regard for image similarity or dissimilarity.

These figures exhibit the diminishing returns of completeness as more images are collected. This effect visually shows how QoI differs from throughput. As seen in these graphs, transmission of successive images does not result in a linear gain in completeness. For example, in Figure 1(b), it is evident that a value of only  $k \approx 10$  is needed to collect 5 images matching the target content, while collecting an additional 2 from the same set usually requires collecting over twice that number of pictures. For comparison, Figure 1(b) also shows the completeness achieved by random selection. Similarly, Figure 1(d) shows that jumping from  $k = 10$  to  $k = 20$ , the likelihood of capturing at least one image of every setting grows substantially from just over 10% to approximately 90%. To approach probabilities close to gaining that final 10%, however, requires a jump to  $k \approx 30$ .

The relationship between the number of images and completeness in each of these graphs also shows that obtaining a certain value of QoI or completeness requires a different number of images depending on the set available and their similarities. We can denote the number of images required to achieve a level of completeness,  $C$ , as  $k_{req} = Q(C)$ . This relationship will be useful later in determining capacity and scalability limits.

### C. Further Discussion of QoI

We have defined and provided examples for a number of ways that completeness can be defined and used to obtain a concrete data requirement from a contextual QoI requirement. Throughout the rest of the paper, we mainly use sum similarity as the completeness metric, but any of the definitions of completeness used here, or any other QoI requirement that can be translated into a data requirement, for that matter, can be used in the formulation in Section IV.

Also, note that QoI and its usage in understanding networks is not exclusive to these metrics and applications. On the contrary, the model used in the capacity and scalability analysis of Section IV is meant to be an in-depth example of this concept. Modifications to account for different data size requirements should be quite straightforward, and extensions to other time-based metrics should be possible with careful extensions to the framework.

Also, while metadata associated with photographs may be useful in obtaining similar goals to those given in this section, relying on such information is problematic because metadata is not guaranteed to be available, and it is not as universally applicable as content-based retrieval. For example, tags describing the image contents would require users to participate by entering this information, which is time-consuming and unreliable. Location and time stamps may be automatically applied by the device allowing an application to filter images accordingly, but these tags often do not account for factors such as the direction of the camera or obstructed views. Content-based processing, though, can be applied to any set of images.

#### IV. QOI SCALABILITY

Given the nonlinear returns of completeness and importance of timeliness outlined in the previous section, we contend that establishing limits of throughput is insufficient. A non-QoI-aware approach ignores very useful information such as how changes in achievable data rates affect the actual utility of information at its destination as well as how changes in one QoI requirement can affect satisfiability of other requirements.

For these reasons, we set the goal of determining the capacity of a network, and relatedly, the scalability achievable with respect to QoI requirements. Previous methods that predict scalability do so by singling out a single bottleneck node and determining when it will be overloaded and drop packets. Here, we are forced to look at end to end flows and determine all contributors to delay, including MAC access, queuing delays, and multi-hop propagation to find the point at which timeliness requirements are violated or traffic load must be reduced thus adversely affecting completeness, leading to a more comprehensive analysis.

##### A. QoI Satisfiability Framework

In order to establish the framework, we examine an arbitrary flow,  $F_1$ , in the network that has a QoI requirement of  $\mathbf{q} = \{C, T\}$ , where  $C$  is the minimum required completeness metric of choice, such as sum similarity as explained above, and  $T$  is the required timeliness. This flow will have a data size requirement, which is given by a chosen QoI function  $Q(C)$ . Using the example application from III, for example,  $Q(C)$  can return the number of images,  $k_{req}$ , required to achieve the requested completeness  $C$ . Assuming each image has an average size of  $I_S$ , then we can also use  $B$  to describe the total number of bits required by the flow,  $B = k_{req} * I_S$ . To match realistic network implications, we assume this data will be transmitted in a series of packets with size  $P_S$  bits each. The

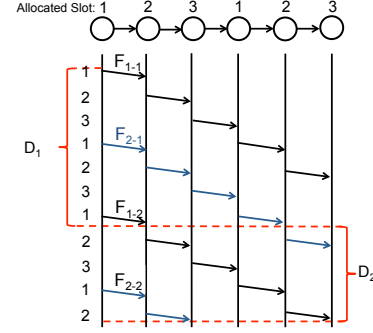


Fig. 2. Example of line network using TDMA highlighting source of delays,  $D_1$  and  $D_2$ . (Node labels are slot assignments.) Here,  $TF = 2$ ,  $CF = 3$ , and  $DF = 1$ .

number of packets per flow, then, is simply  $P_N = \lceil B/P_S \rceil$ . We assume that each node in the network can transmit at  $W$  bits per second when it is allocated media access.

Our goal is to establish the limits at which this arbitrary flow can no longer be completed with the QoI requirements satisfied. We build and explain our model for achieving this goal by working through an example TDMA line network, a portion of which is shown in Figures 2 and 3. (We discuss addressing non-TDMA networks in Section XI.) In this network, we assume a simple 3-slot TDMA scheme, which allows each node equal time access to the medium and removes any potential interference or hidden terminal issues. The TDMA Slot assignments are labeled above each node. For simplicity, we will assume that one slot is appropriately sized to transmit a single packet, i.e.,  $T_{slot} = P_S/W$  and that packets use static routes calculated beforehand such that the overhead is not a consideration here.

Now, two factors,  $D_1$  and  $D_2$ , contribute to the total delay of completing  $F_1$ . The first contributor,  $D_1$ , is the end to end delay incurred by sending the  $B$  bits across the entire path. To quantify this delay, we must consider several factors beyond just the available bandwidth and number of packets. First, each node can only utilize its allotted channel time, creating a Channel Factor of  $CF = N_{frame}/N_i$ , where  $N_i$  is the number of slots allocated to node  $i$  and  $N_{frame}$  is the total number of slots in each frame. In this case,  $N_i = 1, \forall i$  and  $N_{frame} = 3$ .

The second factor to consider for  $D_1$  is the fraction of allocated slots that are utilized by the node to serve flows other than  $F_1$  that are either originating in or being routed through nodes on the path of flow  $F_1$ . We call the total number of flows competing at node  $i$  the Traffic Factor,  $TF_i$ , of that node. For any flow, the maximum contributor to delay is the node along the path with the maximum  $TF_i$ , which we will just call  $TF$  here. More detail about determining this  $TF$  will be outlined in Section V. Incorporating these considerations into a calculation for  $D_1$ , we achieve the following expression:

$$D_1 = T_{slot} \cdot P_N \cdot CF \cdot TF \quad (1)$$

Figure 2 depicts the delay of  $D_1$  in a simple case of only two flows,  $F_1$  and  $F_2$ , being present, in which case  $TF = 2$ .

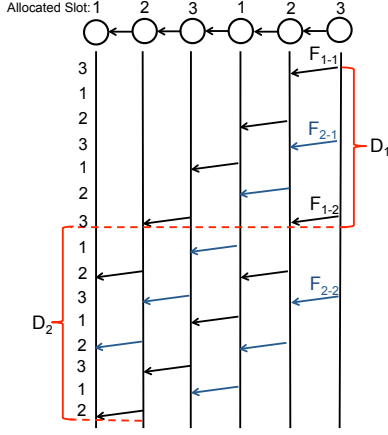


Fig. 3. In the opposite direction,  $DF = 2$ . ( $TF$  and  $CF$  are unchanged here.)

In this example we use flows that consist of only 2 ( $F_{i-j}$  is packet  $j$  in flow  $i$ ) packets to portray the delay. In most real applications,  $P_N$  will be much larger, making  $D_1$  a good approximation of this delay component.

The second delay that exists is due to multi-hop propagation of packets. This delay is simply the time for a single packet to traverse the path length. Note that this delay is not necessarily just the path length multiplied by  $T_{slot}$ , because of possible queuing delays and/or ordering constraints. We show here how ordering constraints impact this TDMA network. A node cannot forward a packet from the flow until it receives that packet from the previous hop. In our line network example, when the direction of the flow matches the nodes' schedule of slots 1 – 2 – 3 – 1 – 2 – 3, as in Figure 2, each successive node receives a packet on the time slot before it is scheduled, resulting in no extra delay. For a flow in the opposite direction, though, where nodes are scheduled 3 – 2 – 1 – 3 – 2 – 1, as in Figure 3, the first slot 1 is not utilized, because the first node scheduled in time slot 1 has not yet received a packet in the flow. Every other slot is wasted, on average, for the initialization of the flow, resulting in approximately twice the delay. We will use a term that we call the *Delay Factor*, or  $DF$ , to account for this effect where it exists. The multi-hop propagation delay, then, is modeled by

$$D_2 = T_{slot} \cdot DF \cdot (PL - 1) \quad (2)$$

where  $PL$  is the average path length.

We note several points about this delay factor. First, in a loaded network, the nodes can and will serve other flows while awaiting the arrival of packets in this flow of focus. That utilized bandwidth does not, however, preclude this  $DF$  impact on delay for the flow of interest,  $F_1$ . Any node cannot serve  $F_1$  until a packet from that flow has been received. Second, this delay is only accounted for once per flow because all other packets are pipelined. All other packets' delay is captured by the end to end delay,  $D_1$ . This effect is best illustrated by examining the difference between  $D_2$  in Figures

2 and 3. Here, we see the multi-hop propagation requires twice the number of slots because every other slot is unused in  $F_1$ 's propagation. To calculate a  $DF$  for an entire network, we can calculate a  $DF$  for each possible sample path and find the average of these values.

By adding the two components of delay, we can give a relation for a network that will successfully achieve an average flow's data and timeliness requirements:

$$T_{slot} \cdot P_N \cdot CF \cdot TF + T_{slot} \cdot DF \cdot (PL - 1) \leq T$$

Recalling that the time of a slot is determined by  $T_{slot} = P_S/W$  and that the total number of bits required for a flow  $P_S \cdot P_N = k_{req} \cdot I_S$  (where  $k_{req}$  is given by a function of required QoI), we can get the following expression:

$$W \cdot T - k_{req} \cdot I_S \cdot CF \cdot TF - P_S \cdot DF \cdot (PL - 1) \geq 0 \quad (3)$$

Every network will have its own set of parameters that can be substituted into this general formula, providing a tool to approximate limitations and sensitivity to changes in specific parameters. To show this usefulness concretely, we provide derived values for a TDMA-based wireless network with several basic topologies.

## V. DEFINING TRAFFIC FACTOR

The Traffic Factor will depend on the traffic pattern and routing scheme used in the network, but here we outline a general formula for modeling it with a random variable. In our formulation, we will focus on an application in which all nodes generate queries that request data of a given size from a randomly chosen destination. We assume that these queries are generated according to a Poisson distribution with an average rate of  $\lambda$ .

Let  $\rho(x)$  be the number of shortest paths of all other nodes that include node  $x$ . Let  $F_{ij}$  represent the existence of a flow existing from node  $i$  to node  $j$ . We assume that  $F_{ij}$  is equal to 1 with probability  $p_f$  and 0 otherwise. Then, the traffic factor of a node  $x$ ,  $TF_x$ , is given by the sum of  $F_{ij}$  for all  $\rho(x)$  pairs  $(i, j)$  in which  $x$  is along the shortest path. Assuming that  $F_{ij}$  is i.i.d. for all pairs  $(i, j)$ , then  $TF_x$  can be approximated by a Normal RV with mean  $\mu_x = \rho(x)p_f$  and variance  $\rho(x)p_f(1 - p_f)$ :

$$f_{TF_x} = \mathcal{N}(\rho(x)p_f, \rho(x)p_f(1 - p_f)) \quad (4)$$

When characterizing the largest contributor to delay, we need to determine the maximum expected Traffic Factor through which the flow will be forwarded. For a given flow from  $i$  to  $j$ , we will use  $TF_{x'|i,j}$  to represent that maximum expected Traffic Factor for that flow, where  $x'$  is given by

$$x' = \arg \max_{x \in \text{Path from } i \text{ to } j} \mu_x \quad (5)$$

More specifically, we can focus on just the distribution of the traffic factor with the maximum mean along the path from  $i$  to  $j$ ,  $f_{TF_{x'|i,j}}$ . We will shorten the notation for this traffic factor distribution to  $f_{TF_{ij}}$ .

## VI. EXAMPLE OF APPLYING FRAMEWORK

We illustrate the application of network signatures to the relationship in (3) using an  $N$ -node TDMA network with three different topologies: clique, line, and grid, also known as a “Manhattan grid.” (Discussion of other network control protocols and topologies are addressed in Section XI.) We adopt a traffic model that uses Top-K queries as an example application. We assume that all nodes have a set of collected images that are used to respond to Top-K queries. Each node produces queries at a rate of  $\lambda$ , each with a target image and target QoI,  $\mathbf{q} = \{C, T\}$ , describing the required completeness (here, we use sum similarity) and timeliness, and sends it to another node chosen at random. The queried node will respond with the required number of images,  $k_{req}$ , according to the empirical relation in Figure 1(a).

For each topology, we must derive an expression of the  $TF$  value.

### A. Line Network Traffic Factor

First, let us look at the number of paths that go through the bottleneck node, which is the center node for a line network. We will assume that  $N$  is odd here, for simplicity of notation, but the logic is the same for even values of  $N$ . Since there are  $\frac{N-1}{2}$  nodes on each side the center node, the total number of paths that go through it is

$$\rho\left(\frac{N}{2}\right) = 2\left(\frac{N}{2} - 1\right)^2$$

Then, since there are  $N$  flows and  $N * (N - 1)$  total paths in the network, we can approximate the probability of each path containing a flow as  $p_f = \frac{1}{N-1}$ . The traffic factor of the center node in a line network can then be approximated by a normal distribution as follows:

$$f_{TF_x} = \mathcal{N}\left(\frac{2\left(\frac{N}{2} - 1\right)^2}{N - 1}, \frac{2\left(\frac{N}{2} - 1\right)^2}{N - 1} \cdot \left(1 - \frac{1}{N - 1}\right)\right)$$

### B. Grid Network Traffic Factor

Again, the bottleneck node, i.e., the node with the highest number of paths going through it is the center node, and we give the derivation for when  $\sqrt{N}$  is odd, but the logic follows similarly for even values. As proved in [18], the most optimal routing scheme for maximum capacity is “Row-First, Column-Second” routing, so we assume paths follow this approach. Again, we adopt a traffic pattern in which each node is the source of exactly one flow and that the destination is uniformly chosen from all other  $N - 1$  nodes. For each source node, we can determine the number of destinations that route through the center. We separate nodes into two categories for this counting.

First, we consider the nodes circled in set  $A$  in Figure 4, of which there are  $\sqrt{N} \cdot \frac{\sqrt{N}-1}{2}$ . Through manual inspection, one can deduce that the only destination nodes in the figure that result in a path that is relayed by the center node are the two bottom nodes in the center column in the figure, marked with blue. There are  $\frac{\sqrt{N}-1}{2}$  of these destination nodes for the

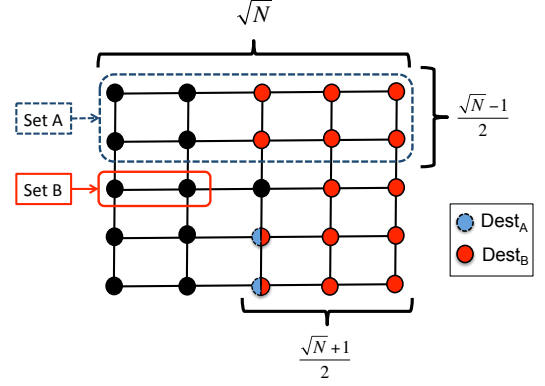


Fig. 4. Sources and destinations used in proving TF for grid networks

nodes in set  $A$ , so the total number of paths from the nodes in set  $A$  is  $\sqrt{N} \cdot \left(\frac{\sqrt{N}-1}{2}\right)^2$ . Now, if we also consider the reverse, i.e. imagine the figure rotated vertically, then we can give the total number of paths from nodes not in the same row as the center node as  $2 \cdot \sqrt{N} \cdot \left(\frac{\sqrt{N}-1}{2}\right)^2$ .

Next, we consider the nodes in the same row as the center node, which we call set  $B$ . Here, all destinations on the “opposite” side of the center as well as those in the same column of the center require being routed through the center node when originating from any nodes in set  $B$ . Just as above, we can count the number of paths from the nodes in set  $B$  that route through the center and double it to count the reverse. The resulting number of paths is  $2 \cdot \left(\sqrt{N} \cdot \frac{\sqrt{N}+1}{2} - 1\right) \cdot \left(\frac{\sqrt{N}-1}{2}\right)$ .

Adding together these paths and simplifying gives us the following expression for the total number of paths that go through the center node:

$$\rho\left(\frac{N}{2}\right) = \sqrt{N} \cdot (N - 2) + 1 \quad (6)$$

Just as with line networks, the probability of each path containing a flow is  $p_f = \frac{1}{N-1}$ , so the traffic factor for the center node of a grid network is given by the distribution:

$$f_{TF_x} = \mathcal{N}\left(\frac{\sqrt{N} \cdot (N - 2) + 1}{N - 1}, \frac{\sqrt{N} \cdot (N - 2) + 1}{N - 1} \cdot \left(1 - \frac{1}{N - 1}\right)\right)$$

which can be approximated by the following for large values of  $N$ .

$$f_{TF_x} = \mathcal{N}\left(\sqrt{N}, \sqrt{N} \cdot \left(1 - \frac{1}{N - 1}\right)\right)$$

### C. Model Equations

Once an expression for the  $TF$  is derived, we can use it along with expressions for  $CF$ ,  $DF$ , and  $PL$  for the network to create equations that estimate the scalability and QoI-satisfiability limits of the network. Since our goal is to determine the point at which the system is unable to support the offered traffic load within the timeliness constraints, we use maximum values for these factors where applicable, specifically  $TF_{max}$  and  $PL_{max}$ .

The  $PL_{max}$  is usually quickly determined by an examination of the topology, such as  $PL_{max} = N - 1$  for a line



network and  $PL_{max} = 2 \cdot \sqrt{N}$  for a grid network. To get a good estimate of  $TF_{max}$ , we can simply utilize the mean and standard deviation of the distribution derived above to create the following:  $TF_{max} = TF_{\mu} + \eta \cdot TF_{sigma}$  where  $\eta$  is a factor that can adjust how conservative the estimates should be. For example, we use  $\eta = 3$ , which captures the 99.7% of the maximum of the distribution. NOTE: Here,  $\eta$  is similar to a z-score of a standard normal distribution. Should we relate it to that to make it more clear?

Table I shows expressions for clique, line, and grid networks as derived above and in [1]. Then, substituting the factors into equation 3, we achieve the scalability equations for each topology in Table II.

	$CF$	$TF_{\mu}$	$TF_{\sigma}$	$DF$	$PL_{max}$
<b>Clique</b>	$N - 1$	1	1	1	1
<b>Line</b>	3	$\frac{2(\frac{N}{2}-1)^2}{N-1}$	$\sqrt{\frac{2(\frac{N}{2}-1)^2}{N-1} \cdot (1 - \frac{1}{N-1})}$	1.5	$N - 1$
<b>Grid</b>	5	$\sqrt{N}$	$\sqrt{\sqrt{N} \cdot (1 - \frac{1}{N-1})}$	2.5	$2 \cdot \sqrt{N}$

TABLE I  
CF, TF, DF, AND PL VALUES FOR EXAMPLE TOPOLOGIES

To find the limitation of a particular parameter or QoI component, the scalability equation can be solved for the variable of interest. Then all known values can be substituted to get the limit of the variable of interest. For example, given a network size and completeness requirement, we can determine a clique network's minimum sustainable timeliness with the equation  $T \geq \frac{I_S \cdot k_{req} \cdot (N-1)}{W}$ , where  $k_{req}$  is given by the completeness function  $Q(C)$ . In practice, solutions for these equations will most likely need to be made numerically, but doing so is rather straightforward using any number of commonly available tools. As we will show in Section IX, these equations can also be easily used to determine the impact of other network parameters on this timeliness limit.

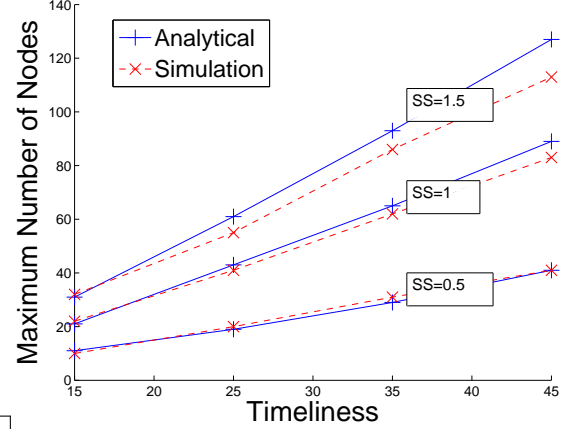
## VII. VALIDATION

To show how effective estimates using this framework can be, we simulated the network topologies and traffic described above in Section VI in the ns3 network simulator, comparing empirical results to those generated analytically with this framework, labeled *Analytical*. We use a channel rate of  $W = 2Mbps$ , packet sizes of  $P_s = 1500$  bytes, and image sizes of 36 and 72 Kbytes. As above, the correlation between Sum Similarity and  $k_{req}$  is taken from the actual observed relation in Figure 1(a). All values of parameters ( $SS$ ,  $T$ ,  $I_S$ , etc.) were chosen to test a variety of network sizes and QoI requirements while remaining within realistic network sizes, both with respect to real-world deployments and simulations with feasible run-times.

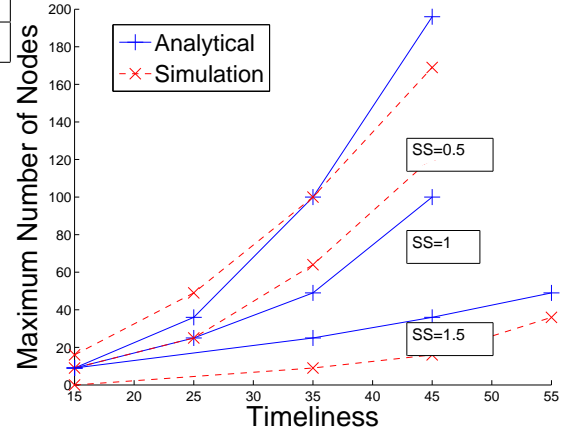
## VIII. FINDING LIMITS AND CHARACTERIZING DELAY

As explained in Section III, delay of a flow can be expressed as

$$D = \frac{k_{req} \cdot I_S \cdot CF \cdot TF}{W} + \frac{P_S \cdot DF \cdot (PL - 1)}{W} \quad (7)$$



(a) Line Network,  $I_S = 18KB$



(b) Grid Network,  $I_S = 48KB$

Fig. 5. Empirical results match analytical results closely for all tests.

We will make some substitutions to get the following version

$$D = \frac{P_S \cdot CF \cdot P_N \cdot TF}{W} + \frac{P_S \cdot DF \cdot (PL - 1)}{W} \quad (8)$$

Building on this equation for delay, we will use the following equation to describe the delay from  $i$  given a destination of  $j$ :

$$D_{i|j} = \frac{P_S \cdot CD \cdot P_N \cdot TF_{i|j}}{W} + \frac{P_S \cdot DF \cdot (PL(i, j) - 1)}{W} \quad (9)$$

Here, we use  $PL()$  as a function that provides the path length between  $i$  and  $j$ . We also assume that  $P_N$  is a random variable that describes the number of packets in a given request, capturing both the possible randomness of  $k_{req}$  and  $I_S$ . Also, recall that  $TF$  is a random variable of the flows being forwarded at the bottleneck node along the path of the flow. Let us define two constants to simplify the expression:

$$C_1 = \frac{P_S \cdot CF}{W}$$

$$C_2 = \frac{P_S \cdot DF}{W}$$

	Equation
<b>Clique</b>	$W \cdot T - I_S \cdot k_{req} \cdot (N - 1) \geq 0$
<b>Line</b>	$W \cdot T - 3 \cdot I_S \cdot k_{req} \cdot (\frac{2(\frac{N}{2}-1)^2}{N-1} + 3 \cdot \sqrt{\frac{2(\frac{N}{2}-1)^2}{N-1} \cdot (1 - \frac{1}{N-1})}) - 1.5 \cdot P_S \cdot (N - 1) \geq 0$
<b>Grid</b>	$W \cdot T - 5 \cdot I_S \cdot k_{req} \cdot (\sqrt{N} + 3 \cdot \sqrt{\sqrt{N} \cdot (1 - \frac{1}{N-1})}) - 2.5 \cdot P_S \cdot (\frac{2}{3}\sqrt{N} - 1) \geq 0$

TABLE II  
SCALABILITY EQUATIONS

Then, we can express the delay as

$$D_{i|j} = C_1 \cdot P_N \cdot TF_{i|j} + C_2 \cdot PL(i, j) \quad (10)$$

We can develop the following expression for a distribution of delay:

$$\begin{aligned}
P(D_{i|j} \leq d) &= P(C_1 \cdot P_N \cdot TF_{i|j} + C_2 \cdot PL(i, j) \leq d) \\
&= P(P_N \cdot TF_{i|j} \leq \frac{d - C_2 \cdot PL(i, j)}{C_1}) \\
&= \sum_{tf=1}^{tf_{max}} P(P_N \cdot TF \leq \frac{d - C_2 \cdot PL(i, j)}{C_1} | TF = tf) \cdot f_{TF_{i|j}}(tf) \\
&= \sum_{tf=1}^{tf_{max}} P(P_N \leq \frac{d - C_2 \cdot PL(i, j)}{C_1 \cdot tf}) \cdot f_{TF_{i|j}}(tf) \\
F_{D_{i|j}}(d) &= \sum_{tf=1}^{tf_{max}} F_{P_N}(\frac{d - C_2 \cdot PL(i, j)}{C_1 \cdot tf}) \cdot f_{TF_{i|j}}(tf)
\end{aligned}$$

Then, we can generalize the expression to give a distribution for a flow originating in node  $i$  with an unknown destination by conditioning over all possible destinations,  $j$ .

$$F_{D_i} = \sum_{j \neq i} [\sum_{tf=1}^{tf_{max}} F_{P_N}(\frac{d - C_2 \cdot PL(i, j)}{C_1 \cdot tf}) \cdot f_{TF_{i|j}}(tf)] \cdot p(j) \quad (11)$$

Finally, we can get an average distribution of all flows' delays by summing over all sources and dividing by the the number of sources. This average delay distribution is in Equation (11).

#### A. Minimum Timeliness/Maximum Query Rate

The first useful information that can be gathered from the delay distribution is the maximum expected delay,  $d_{max}$ , of a flow in the network, which occurs at the delay  $d$  at which  $F_D$  reaches its maximum value of 1. If the average rate of queries,  $\lambda$ , is greater than  $\frac{1}{d_{max}}$ , then the traffic will exceed the network capacity and the number of active queries in the system will grow without bound, causing packets to be dropped and/or delays to grow without bound. Therefore, the maximum query rate is  $\lambda_{max} = \frac{1}{d_{max}}$ , and, consequently, the minimum timeliness for which *all* flows can be expected to complete before the deadline is  $d_{max}$ .

In some applications, having a certain amount of queries not complete by the timeliness requirement may be acceptable. In these situations, more useful information can be extracted from the delay distribution in Equation (12). Specifically, this delay

distribution can be interpreted as the expected percentage of queries that will finish within the timeliness constraint if the timeliness constraint was  $d$ . As we will show in Section VI, this relationship follows a Normal distribution CDF.

#### B. Probability of Timeliness Satisfiability

While the minimum timeliness at which all flows are expected to complete before their deadlines can be determined by the scalability equations in Section VI, some applications may benefit from an understanding of what the probability of completing within the timeliness constraints for those below the minimum fully satisfiable timeliness. For example, if a mission issues a number of queries for information to support decision-making, receiving 80% or 90% of the responses may be sufficient for making the decision. The question of importance, then, is "How far can we reduce the timeliness constraint and still expect to receive  $x\%$  of the queries in time?" Or, equivalently, we may pose the question, "When the network is operating at the edge of capacity, what is the expected delay for  $x\%$  of queries to be completed?" Since equation 12 provides the distribution of delays, it provides quality estimates to answer these questions.

Figure 6 shows expected delay distributions from 12 alongside distributions of delays recorded in ns3 simulations of the same networks. In all cases, above 0.5 probability analytical predictions are within about 10% of empirical results. We believe this end of the distribution provides much more useful information since minimum QoI requirements for most applications tend to be over 50%. However, in smaller data load requirement cases, analytical predictions match simulation results quite closely along the entire distribution.

### IX. IMPACT ON NETWORK DESIGN

Now that we have established a model for QoI satisfiability and scalability and shown its accuracy in predicting estimated limits, we show how it can also provide quick, but useful intuition about the impact of various network parameters. Once an equation for a network's limitations is formulated as was done for equations in Table II, it can be solved for a single parameter to gain an understanding of its reliance on the other factors. This analysis can be done very quickly and easily by approximating when appropriate, or by using symbolic and/or numerical solvers. To exemplify this application in network design, we have applied this process to the equations in Table II and created several figures that provide insight into network limitations and tradeoffs.

Figure 7(a) shows minimum satisfiable timeliness values for different topologies of increasing size. While it may be



$$F_D(d) = \frac{1}{N} \cdot \sum_{i=1}^N \sum_{j \neq i} \sum_{tf=1}^{tf_{max}} F_{PN} \left( \frac{d - C_2 \cdot PL(i, j)}{C_1 \cdot p_N} \right) \cdot f_{TF_{i|j}}(tf) \cdot p(j) \quad (12)$$

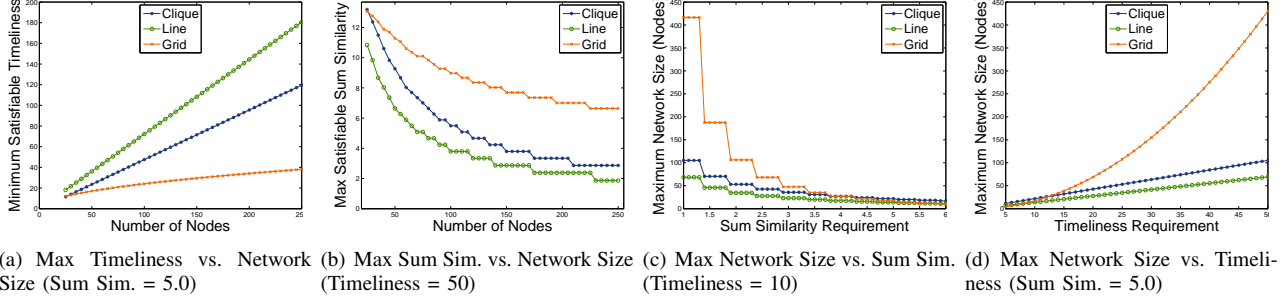
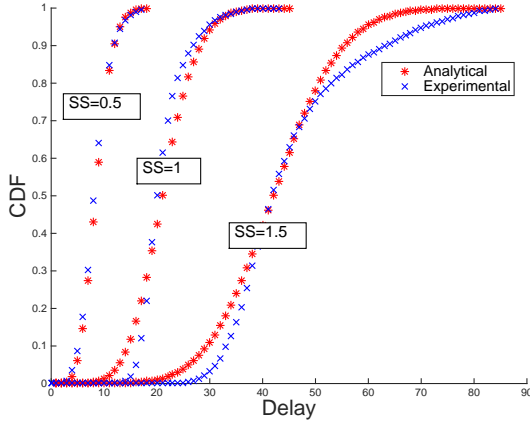
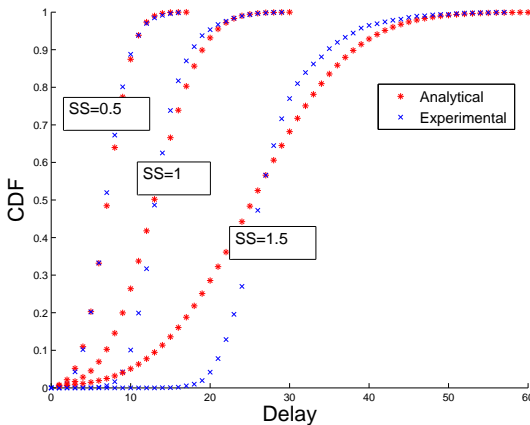


Fig. 7. Varying design parameters provide immediate limitations as well as evident trends and comparisons.



(a) Line Network,  $N = 40$ ,  $I_S = 36KB$



(b) Grid Network,  $N = 49$ ,  $I_S = 72KB$

Fig. 6. Characterization of delay using framework follows distribution of empirical results in most cases.

intuitive that a grid network should be able to serve flows with lower timeliness constraints than a line network since it will have shorter average path lengths, what is not intuitive is *how much* lower of a timeliness constraint is satisfiable. Here, we see that a grid network can scale up to over 250 nodes while supporting flows with  $T = 40$ . A line network, on the other hand, can only scale to only approximately 20% of that network size for the same timeliness value.

Figure 7(b) visualizes sum similarity limits for network instances with timeliness fixed. Here, again, limits and trends are quickly evident. In addition, the nonlinearity of completeness requirements are manifested here as the data requirements for the highest completeness requirements are only sustainable for small networks, but as the network size increases, the impact on achievable completeness is not as dramatic.

Finally, given a topology and application with predetermined requirements of  $\mathbf{q}$ , we may be simply interested in how large our network can grow before its capacity to deliver the desired QoI is no longer possible. Values that answer this question are in Figures 7(c) and 7(d). Once again, the graphs show the major impact completeness and timeliness requirements can have on network size. Figure 7(c) especially shows the impact of using completeness instead of simply throughput as the non-linear relationship of completeness to data rate pointed out in Section III is evident here.

## X. SCALABLY FEASIBLE QOI REGIONS

Now let us consider a special case where nodes collect a total of  $k_{req}$  images, but each image must come from a different node, perhaps because each node only has one image or maybe by design to provide increased credibility through corroboration, another contextual metric of interest in QoI-aware networks. This scenario allows us to illustrate an interesting observation.

Consider a set of QoI requirements that include completeness and timeliness,  $\mathbf{q} = \{C, T\}$ . As previously noted, a certain number of images are required to achieve this desired level of completeness,  $Q(C) = k_{req}$ . Unlike the model used in Section IX, however, each node can contribute only one image to  $k_{req}$ , which implies a minimum network size of

$N \geq k_{req}$  in order to achieve the completeness outlined in the QoI requirements. On the other hand, applying the framework of Section IV to this network, we can determine the maximum network size, which we will call  $N_{max}$  here for distinction.

These two facts are important, because when  $N_{max} < k_{req}$ , then it is not possible to provide the QoI level  $\mathbf{q}$ . Hence, this set of QoI requirements is infeasible, or *scalably infeasible*. This phenomenon defines the concept of a *Scalably Feasible QoI Region*, which refers to the region in which all sets of QoI pairs can be supported with the given network signature.

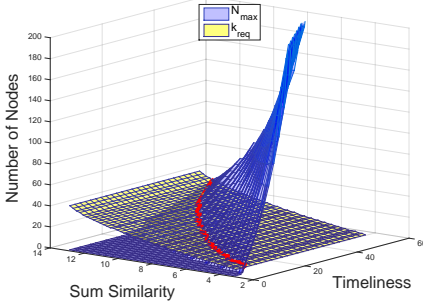


Fig. 8. The blue plane represents maximum scalability, and the yellow plane represents minimum required images. Therefore, all (Sum Sim., Timeliness) pairs to the right of the red line are within the scalably feasible QoI region.

Figure 8 provides a visual representation of this region for a grid network that institutes the given traffic model assuming traffic is routed over randomly chosen shortest-path routes. Here,  $N_{max}$ , calculated for  $\mathbf{q}$  pairs from  $\{2.5, 1\}$  to  $\{13.0, 50\}$ , is shown in the graph by the blue surface. On the same graph is the number of images required,  $k_{req}$ , for each Sum Similarity requirement, shown with the yellow surface on the graph. The intersection of these two surfaces, displayed with a red line, provides the edge of the scalably feasible QoI region. In this example, all sum QoI pairs to the right of this line, i.e. the region where  $N_{max} > k_{req}$ , are scalably feasible.

In general, regardless of how many images a node has, it is possible to analyze the trade-off between different QoI attributes for a fixed value of maximum network size,  $N_{max}$ . Specifically, by fixing  $N$  in Table II, one can obtain  $T$  and  $k_{req}$  (and, hence,  $C$ ) resulting in the set of supportable  $\{C, T\}$  pairs defining a feasible region for QoI. This region can be visualized by intersecting the blue scalability curve with a flat surface fixed at  $N_{max}$  instead of the yellow surface in Figure 8. The scenario given in this section goes one step further and also takes into account the network size actually required to generate/support a given QoI requirement (using the non-flat yellow surface derived from experimental results in Figure 8).

## XI. DISCUSSION

We note that although TDMA is primarily used in this work, the same approach can be taken to derive QoI-based relations in networks that use other MAC layer protocols. In these cases, the appropriate Delay Factor would need to be derived for each protocol. To examine an 802.11 network, for example, the  $DF$  would capture queuing delays and could be determined by extending a delay model such as in [19], for example.

Similarly, although we only address the regular topologies of clique, line, and grid networks here, we believe the framework can be applied to more complex, irregular network topologies. In fact, some of the simple models presented here may already be quite useful for some of the topologies addressed. As shown in [20], for example, a dense random network may be closely approximated by a clique network, or random networks' capabilities can be approximately bounded by the limits of clique and grid networks, since these networks can be viewed of as examples of dense and sparse random networks, respectively.

## XII. CONCLUSION

This work provides several contributions to the field of QoI-aware wireless networks. First, we motivated the use of completeness and timeliness as QoI attributes, providing an example application and several different ways to measure completeness. Next, we developed a framework that can be used to predict QoI and network size limits for a specific network and then validated the framework's accuracy by comparing analytical results with simulations performed in the ns3 network simulator. Examples of the impact of different network parameters were shown, providing concrete examples of the framework's usefulness in real-world applications. In addition, the concept of scalably feasible QoI regions was introduced. For future work, we plan to make generalizations of factors that will allow for easy application of this framework to any non-regular network topology as well as extend the framework to predict performance and scalability of networks with flexible QoI requirements.

## APPENDIX A

### EXPLANATION OF EXPECTED QOI WITH RANDOM IMAGE SELECTION

#### A. Top-K

First, we explain the expected number of images that are from the same set as the target image in the Top-K algorithm when images are selected from the entire image pool at random. We define the following:

- $n$  = total number of images (summed over all sets)
- $S$  = number of sets
- $S_k$  = set of target image
- $k$  = number of images selected
- $N_S$  = number of images in each set (for simplicity, assumed to be the same for all sets)
- $x$  = number of images returned from set  $S_k$

$$P(X = x|k) = \begin{cases} \frac{\binom{k}{x} * \binom{n-k}{k-x}}{\binom{n}{k}} & \text{if } k \leq N_S, \\ \frac{\binom{N_S}{x} * \binom{n-N_S}{k-x}}{\binom{n}{k}} & \text{if } N_S < k \leq n - N_S \end{cases} \quad (13)$$

Equation 13 provides the probability that  $x$  of the  $k$  selected images will be from the target set. When  $k \leq N_S$ , the total

number of possible combinations of choosing  $x$  from the target set and  $k - x$  from the  $n - N_{S_k}$  remaining images over the entire sample space ( $n$  choose  $k$ ). When  $N_S < k < n - N_S$ , then we consider the possible combinations of choosing  $x$  images from the target set and  $k - x$  images from the remaining  $n - N_S$  images. This probability formula can then be used to derive the expected values of  $x$  displayed in Figure 1(b).

### B. Clustering

For Clustering, we want to determine the probability that we will cover each of the  $S$  sets with at least one of the  $k$  chosen images if we had chosen them randomly. We will call  $X_i$  the random variable that represents the number of images from set  $i$  in the results. We use the following expression:

$$P(X_i > 0, \forall i|k) = (1 - P(X_i = 0))^S \quad (14)$$

where  $X_i$  is given by a multivariate hypergeometric distribution, which gives us the following:

$$P(X_i = 0|k) = \frac{\binom{n-N_s}{k}}{\binom{n}{k}} \quad (15)$$

This probability expression is plotted directly against the percentage of trials in which all sets were covered in experiments using the Clustering algorithm in Figure 1(d).

### REFERENCES

- [1] R. Ramanathan, E. Ciftcioglu, A. Samanta, R. Uргаonkar, and T. La Porta. Symptotics: a framework for estimating the scalability of real-world wireless networks. *Wireless Networks*, 2016. to appear, available online at <http://link.springer.com/article/10.1007/s11276-016-1204-4>.
- [2] R. Ramanathan, A. Samanta, and T. La Porta. Symptotics: A framework for analyzing the scalability of real-world wireless networks. In *Proceedings of the 9th ACM symposium on PE-WASUN*, pages 31–38. ACM, 2012.
- [3] E.N. Ciftcioglu, R. Ramanathan, and T.F. La Porta. Scalability analysis of tactical mobility patterns. In *MILCOM 2013*, pages 1888–1893. IEEE, 2013.
- [4] J. Li, C. Blake, D. SJ De Couto, Hu Imm Lee, and R. Morris. Capacity of ad hoc wireless networks. In *Proceedings of the 7th annual international conference on Mobile computing and networking*, pages 61–69. ACM, 2001.
- [5] P. Gupta and P.R. Kumar. The capacity of wireless networks. *Information Theory, IEEE Transactions on*, 46(2):388–404, 2000.
- [6] A. I Khuri and S. Mukhopadhyay. Response surface methodology. *Wiley Interdisciplinary Reviews: Computational Statistics*, 2(2):128–149, 2010.
- [7] H. Tan, M. Chan, W. Xiao, P. Kong, and C. Tham. Information quality aware routing in event-driven sensor networks. In *IEEE INFOCOM, 2010*, pages 1–9, 2010.
- [8] Z. M. Charbiwala, S. Zahedi Y. Kim, Y.H. Cho, and M. B. Srivastava. Toward Quality of Information Aware Rate Control for Sensor Networks. In *Fourth International Workshop on Feedback Control Implementation and Design in Computing Systems and Networks*, April 2009.
- [9] E.N. Ciftcioglu, A. Yener, and M.J. Neely. Maximizing quality of information from multiple sensor devices: The exploration vs exploitation tradeoff. *Selected Topics in Signal Processing, IEEE Journal of*, 7(5):883–894, Oct 2013.
- [10] J. Edwards, A. Bahjat, Y. Jiang, T. Cook, and T.F. La Porta. Quality of information-aware mobile applications. *Pervasive and Mobile Computing*, 11:216–228, 2014.
- [11] E. N. Ciftcioglu, A. Michaloliakos, A. Yener, K. Psounis, T. F. La Porta, and R. Govindan. Operational information content sum capacity: From theory to practice. *Computer Networks*, 75:1–17, 2014.
- [12] E. N. Ciftcioglu, A. Michaloliakos, K. Psounis, T. F. La Porta, and A. Yener. Power minimization with Quality-of-Information Outages. In *Proc. IEEE WCNC*, Istanbul, Turkey, April 2014.
- [13] M.Y.S. Uddin, H. Wang, F. Saremi, G.-J. Qi, T. Abdelzaher, and T. Huang. Photonet: a similarity-aware picture delivery service for situation awareness. In *Real-Time Systems Symposium (RTSS), 2011 IEEE 32nd*, pages 317–326. IEEE, 2011.
- [14] Y. Jiang, X. Xu, P. Terlecky, T. Abdelzaher, A. Bar-Noy, and R. Govindan. Mediascope: selective on-demand media retrieval from mobile devices. In *Proceedings of the 12th international conference on Information processing in sensor networks*, pages 289–300. ACM, 2013.
- [15] A. Bar-Noy, G. Cirincione, R. Govindan, S. Krishnamurthy, T.F. LaPorta, P. Mohapatra, M. Neely, and A. Yener. Quality-of-information aware networking for tactical military networks. In *Pervasive Computing and Communications Workshops (PERCOM Workshops), 2011 IEEE International Conference on*, pages 2–7. IEEE, 2011.
- [16] S.A. Chatzichristofis and Y.S. Boutalis. Cedd: color and edge directivity descriptor: a compact descriptor for image indexing and retrieval. In *Computer Vision Systems*, pages 312–322. Springer, 2008.
- [17] T.T. Tanimoto. An elementary mathematical theory of classification and prediction. *International Business Machines Corporation*, 1958.
- [18] Guillermo Barrenechea, Baltasar Beferull-Lozano, and Martin Vetterli. Lattice sensor networks: Capacity limits, optimal routing and robustness to failures. In *Information Processing in Sensor Networks, 2004. IPSN 2004. Third International Symposium on*, pages 186–195. IEEE, 2004.
- [19] N. Gupta, P.R. Kumar, et al. A performance analysis of the 802.11 wireless lan medium access control. *Communications in Information & Systems*, 3(4):479–304, 2003.
- [20] R. Ramanathan, Ciftcioglu E., A. Samanta, Uргаonkar R., and T.L. Porta. An approximate model for analyzing real-world wireless network scalability. Technical report, Raytheon BBN Technologies, 2015. <http://www.ir.bbn.com/~ramanath/pdf/symptotics-techreport.pdf>.